

Robust Learning via Persistency of Excitation

Kaustubh Sridhar Oleg Sokolsky Insup Lee James Weimer
University of Pennsylvania
{ksridhar, sokolsky, lee, weimerj}@seas.upenn.edu

Abstract

Improving adversarial robustness of neural networks remains a major challenge. Fundamentally, training a network is a parameter estimation problem. In adaptive control theory, maintaining persistency of excitation (PoE) is integral to ensuring convergence of parameter estimates in dynamical systems to their robust optima. In this work, we show that network training using gradient descent is equivalent to a dynamical system parameter estimation problem. Leveraging this relationship, we prove a sufficient condition for PoE of gradient descent is achieved when the learning rate is less than the inverse of the Lipschitz constant of the gradient of loss function. We provide an efficient technique for estimating the corresponding Lipschitz constant using extreme value theory and demonstrate that by only scaling the learning rate schedule we can increase adversarial accuracy by up to 15% points on benchmark datasets. Our approach also universally increases the adversarial accuracy by 0.1% to 0.3% points in various state-of-the-art adversarially trained models on the AutoAttack benchmark, where every small margin of improvement is significant.¹

1 Introduction

Neural networks are vulnerable to adversarial examples [Szegedy et al., 2013, Biggio et al., 2013] and earlier works [Carlini and Wagner, 2017, Athalye et al., 2018] have shown that most existing defenses are still highly susceptible to white box attacks (where the adversary has full access to the network and its defense mechanism). An exception, Projected Gradient Descent (PGD) based Adversarial Training (PGD-AT) [Madry et al., 2017] and its variants [Zhang et al., 2019, Carmon et al., 2019, Uesato et al., 2019, Sitawarin et al., 2020, Rice et al., 2020, Pang et al., 2020a, Chen et al., 2020, Wang et al., 2019, Schwag et al., 2020, 2021, Pang et al., 2020b, Wu et al., 2020, Zhang et al., 2020, Wu et al., 2021] are considered the most successful attempts at creating a defense to white-box attacks. But, with adversarial accuracies in the range of 40% to 60% on the AutoAttack² benchmark [Croce and Hein, 2020], they still have room for improvement.

We believe that adversarial robustness can be improved by leveraging the fact that every neural network training process (standard or robust) is a parameter estimation problem [Nar and Sastry, 2019], where the goal is to find the true parameters of a model. The parameters corresponding to a local optima at a flat region of a model’s loss-landscape are thought to belong to a robust optima of the model [Wu et al., 2020, Chaudhari et al., 2019]. Our intuition is that a true set of model parameters, where similar inputs always map to similar outputs, would lie at a model’s robust optima.

In adaptive control theory, persistency of excitation (PoE) conditions [Sastry and Bodson, 2011, Ioannou and Sun, 2012, Narendra and Annaswamy, 2012] have been proven to be integral to robust parameter estimation. Further, recent work [Nar and Sastry, 2019] analyzed neural network training and identified the lack of PoE in gradient descent as a major roadblock on the path to robustness.

¹Code: <https://github.com/kaustubhsridhar/PoE-robustness>

²A leaderboard can be found at <https://robustbench.github.io/>

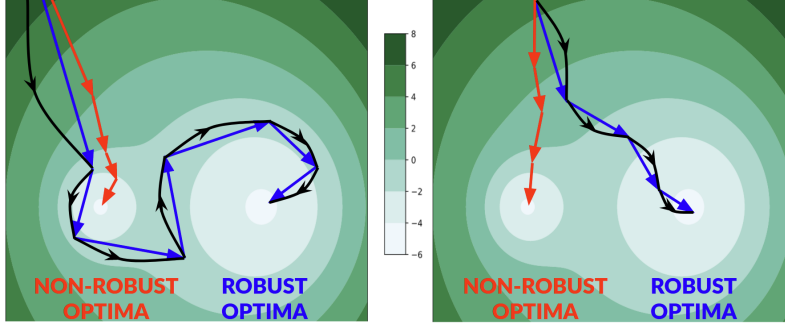


Figure 1: Intuition: Two illustrations where gradient descent updates (blue arrows) that lie on persistently exciting trajectories (black curves) go to robust optima whereas, a typical learning rate (lr) schedule starting at an initial value of 0.1 (red arrows) leads to local but not robust optima.

PoE conditions restrict parameter estimation dynamics to exponentially-stable trajectories that ensure robust convergence to true values. With our intuition of true parameters coinciding with a robust optima, constraining training dynamics to a persistently exciting trajectory should (and does in our experiments) lead to increased robustness in both standard and robust learning. Our intuition is depicted on two illustrative loss-landscapes in Figure 1. Thus, the main challenge addressed by this work is ensuring the training dynamics follows a persistently exciting trajectory – which we prove can be achieved by only adjusting the learning schedule.

Specifically, in this work, we find sufficient conditions for every pair of consecutive updates of gradient descent to lie on a persistently excited trajectory. These sufficient conditions are equivalent to scaling a baseline learning schedule. Our novel approach to this problem provides a guarantee for PoE of all models trained by gradient descent. Earlier attempts to characterize PoE for gradient descent were either impeded by a neural network’s inherent nonlinearities [Lu and Basar, 1998, Polycarpou and Ioannou, 1991] or limited to simple two layer networks and specific loss functions [Nar and Sastry, 2019].

Further, in our approach, the initial value of the scaled learning rate schedule for PoE is a function of the inverse of Lipschitz constant of the loss gradient. To ensure a rigorous evaluation with minimal increase in model training time, we estimate this second-order Lipschitz constant with an inexpensive addition to the baseline model training procedure via extreme value theory [Wood and Zhang, 1996, De Haan and Ferreira, 2007, Weng et al., 2018].

To observe the utility of our persistently exciting learning schedule, we apply it to both standard training on MNIST [LeCun, 1998], CIFAR10, CIFAR100 [Krizhevsky et al., 2009] datasets, and adversarial training on CIFAR10 dataset. We see an increase in adversarial accuracy of upto 15% points against a 20-step PGD adversary with perturbation budget $\epsilon = 1/255$ in standard training and an increase of 0.1% to 0.3% points on the Autoattack benchmark (with $\epsilon = 8/255$) composed of both white-box and black-box attacks, where based on the leaderboard, improvements of 0.04% points are considered significant. Our contributions can be summarized as follows:

- To the best of our knowledge, we describe a novel method to analyze gradient descent through a robust parameter estimation lens.
- We leverage our methodology to derive sufficient conditions for PoE in gradient descent. These conditions are both model and loss function agnostic but depend on gradient descent dynamics. Even so, when training in practice with stochastic gradient descent (SGD) rather than gradient descent, we demonstrate that they aid robustness.
- We present an efficient implementation strategy, based on extreme value theory, to obtain an estimate of an initial learning rate in a learning schedule for PoE. Using this, we are able to train standard models with better white-box l_∞ -adversarial accuracy than those obtained via baseline training on MNIST, CIFAR10, and CIFAR100 datasets (upto 15% points increase against 20-step PGD attack with perturbation budget $\epsilon = 1/255$).
- Our approach results in increased l_∞ -robustness (adversarial accuracy increase of 0.1% to 0.3% points) in various state-of-the-art (SOTA) adversarially trained models on CIFAR10 on the highly-competitive Autoattack benchmark (with $\epsilon = 8/255$), where improvements of 0.04% points are considered significant.

2 Related Work

Robust learning has been explored in a large body of work. PoE has also enjoyed an expansive exploration in control theory literature. Here, we only discuss papers relevant to our approach.

Techniques for Robust Learning. Adversarial training (AT), first introduced in [Goodfellow et al., 2014] and currently, the most effective defense to white-box attacks, requires solving a min-max optimization problem. The inner maximization problem is approximately solved with the PGD attack in (PGD-AT) [Madry et al., 2017]. A variant of the same that modifies the inner maximization problem to tradeoff clean accuracy for robust accuracy was proposed in (TRADES) [Zhang et al., 2019]. Parallely, unlabelled data was shown to aid TRADES in (RST) [Carmon et al., 2019] and PGD-AT in (UAT) [Uesato et al., 2019]. PGD-AT and TRADES were further improved upon with early stopping (ATES) [Sitawarin et al., 2020, Rice et al., 2020], batch normalization layers set to evaluation mode [Pang et al., 2020a], pre-training [Hendrycks et al., 2019, Chen et al., 2020], revisiting mis-classified examples (MART) [Wang et al., 2019], assimilating proxy distributions [Sehwag et al., 2021], pruning (HYDRA) [Sehwag et al., 2020], incorporating a hypersphere embedding [Pang et al., 2020b], weight loss-landscape and logit smoothing [Wu et al., 2020, Chen et al., 2021], geometry based model re-weighting (GAIR) [Zhang et al., 2020], and wider networks (Wide-RST) [Wu et al., 2021].

Of all of the above, Wide-RST [Wu et al., 2021] performs the best on the AutoAttack benchmark, *a.k.a.* RobustBench (an ensemble of four white-box and black-box attacks with a single hyperparameter - perturbation budget $\epsilon = 8/255$) [Croce and Hein, 2020]. Wide-RST is based on another SOTA approach from 2019: namely, RST [Carmon et al., 2019] which is in-turn built upon TRADES [Zhang et al., 2019]. **Applying our approach improves the robustness of all these three SOTA methods.** Our approach also improves upon the original adversarial training method PGD-AT [Madry et al., 2017]. We consider our approach to act as a force-multiplier- it improves the robustness of any existing model whether obtained by standard or adversarial training.

PoE in Control Theory and Deep Learning. PoE, first introduced in [Åström and Torsten, 1965], has been thoroughly explored for continuous-time (CT) linear time-varying (LTV) systems in control theory literature. This concept is essential to robust parameter estimation in guaranteeing global exponential stability (GES) of parameter error dynamics which in turn ensures convergence of estimated parameters to the true values [Sastry and Bodson, 2011, Ioannou and Sun, 2012, Narendra and Annaswamy, 2012, Sukumar and Akella, 2012]. For learning-based system identification, early work [Gorinevsky, 1995, Kurdila et al., 1995] found PoE conditions for Radial Basis Function (RBF) mappings but emphasizes the difficulty in characterizing PoE conditions for general neural network models because of the nonlinearities in the models [Lu and Basar, 1998, Polycarpou and Ioannou, 1991].

Recently, seminal work in Nar and Sastry [2019] aim to tackle this challenging problem. Based on the premise of robust neural networks having bounded Lipschitz constants [Szegedy et al., 2013], they derive sufficient richness conditions on the inputs to a two-layer network with ReLU activation functions trained with gradient descent. However, their results are specific to a two-layer network initialized close to its true optima, and is dependent on the gradient update rule as well as loss function. Moreover, these conditions do not scale to modern deep neural networks. To scale, the authors are forced to adopt an optimization trick to force noise (for PoE) into each layer of a deep neural network. This trick can also be found in other approaches for robust learning [Lecuyer et al., 2019, Cohen et al., 2019, Li et al., 2018].

To avoid falling into the same nonlinearity & complexity trap, we flip the problem around: we start with a well-characterized CT LTV family of persistently excited dynamics and then find sufficient conditions for gradient descent updates to fit on the trajectories in this family. Our approach is only dependent on the gradient update rule and in practice, scales to models that converge in training. Control theorists may draw an analogy from our approach to Model-Reference Adaptive Control (MRAC) [Sastry and Bodson, 2011]. In MRAC, adaptive control laws are chosen such that the system’s dynamics behave like that of a reference system’s dynamics. In our approach, we choose a learning rate schedule such that gradient descent dynamics belong to a PoE family.

3 Problem Formulation

In this section, we mention some preliminaries from control theory and gradient descent in Section 3.1 and then we formally state our problem in Section 3.2.

3.1 Preliminaries

Control Theoretic Preliminaries. Following Section 2, we describe a CT LTV system as,

$$\dot{z}(t) = -\Phi(t)\Phi(t)^T z(t), \quad t \geq 0 \quad (1)$$

with $z(t) \in \mathbb{R}^d$, $\Phi(t) \in \mathbb{R}^{d \times p}$, and the following definition of PoE,

Definition 1 (PoE [Sastry and Bodson, 2011]). The signal $\Phi(t) : \mathbb{R}^{\geq 0} \rightarrow \mathbb{R}^{d \times p}$ is said to be persistently exciting if there exists $\mu_1, \mu_2, T_0 > 0$ such that,

$$\mu_2 \mathbf{I} \geq \int_t^{t+T_0} \Phi(s)\Phi(s)^T ds \geq \mu_1 \mathbf{I} \quad (2)$$

where \mathbf{I} is the $d \times d$ Identity matrix. We can now state the following lemma.

Lemma 1 (PoE and Global Exponential Stability (GES) [Sastry and Bodson, 2011]). If $\Phi(t) \in \mathbb{R}^{d \times p}$ is piece-wise continuous and persistently exciting, then system (1) is GES.

The above lemma informs us that a state trajectory given by (1) converges exponentially fast to its equilibrium. This lemma is integral to defining a family of trajectories for our gradient decent updates to track. Said gradient descent updates are described below.

Gradient Descent Preliminaries. We represent feature space with \mathcal{X} , label space with \mathcal{Y} and model with parameters $\Theta \in \mathcal{P}$ given by $h_\Theta : \mathcal{X} \rightarrow \mathcal{Y}$. In the theoretical part of this work, we focus on model training with gradient descent wherein, we represent the training data with $(X, Y) \in \mathcal{X} \times \mathcal{Y}$ and the loss function minimized with $L : \mathcal{X} \times \mathcal{Y} \rightarrow \mathbb{R}$. We denote the vectorized versions of parameters and loss gradients as $\theta = \text{vec}(\Theta) \in \mathbb{R}^d$ and $\nabla l(\theta) = \text{vec}(\nabla L(h_\Theta(X), Y)) \in \mathbb{R}^d$. We also denote the learning rate with η . Now, we write the gradient descent update step in a vectorized form as follows.

Definition 2 (Vectorized Gradient Descent Update). The vectorized form of the k th update step in gradient descent for training a model h_Θ on training data (X, Y) by minimizing loss $L(h_\Theta(X), Y)$ with learning rate η^k is given by

$$\theta^{k+1} = \theta^k - \eta^k \nabla l(\theta^k), \quad k = 1, 2, \dots \quad (3)$$

The above definition casts gradient descent into a DT NLTV system. Analyzing this system for a particular loss function l and model architecture h_θ is intractable for increasingly deeper and wider models trained by minimizing custom loss functions. We present a top-down solution to handle this problem. Our solution requires us to define a well-characterized family of dynamics and then constrain consecutive states of the DT NLTV system in (3) to lie on trajectories from this family. More details on the chosen family of dynamics can be found in the next subsection.

3.2 Problem Statement

Let us choose a family of persistently exciting dynamics such that all of its members converge exponentially-fast to the unknown true parameters of a model (given by θ^*). Each member of this family, for $k \geq 1$, begins at the k th gradient descent update (θ^k). Such a family is given as follows.

Definition 3 (Family of Persistently Exciting Dynamics). The family of persistently exciting dynamics, with GES equilibrium at θ^* , that governs the evolution of a state vector $\Gamma(t) \in \mathbb{R}^d$, $t \geq k$ with initial value $\Gamma(k) = \theta^k$, is given by

$$\dot{\Gamma}(t) = -\Phi(t)\Phi(t)^T (\Gamma(t) - \theta^*) \quad (4)$$

where $\Phi(t) = \Phi^k \forall t \in [k, k+1)$ is piece-wise constant matrix $\in \mathbb{R}^{d \times p}$ and $\Phi^k \Phi^{k\top}$ is full rank $\forall k$.

Equation (4) is a form of the CT LTV system in (1) with an equilibrium at θ^* . Our choice of $\Phi(t)$ in the above definition ensures that $\Phi(t)$ is persistently exciting and consequently that the system in (1) has GES equilibrium (Proved in Section 4). Finally, with the requisite family defined, we formally state the problem considered by this work below.

Problem Statement 1 (PoE of Models Trained with Gradient Descent). We aim to find sufficient conditions for every pair of consecutive k th-step gradient descent updates θ^k, θ^{k+1} (Definition 2) to lie on a persistently excited trajectory from the family in Definition 3.

4 Learning Rates for PoE

In this section, we present our main theoretical result in Theorem 1 which proposes an upper bound on learning rates η^k , $k \geq 1$ such that our problem statement is accomplished. Also in this section, we provide intuition for relating our result to convex optimization, constant learning rate training, and practical SGD. Before formally stating the theorem, we present our primary assumption on \mathcal{L} -smoothness of the loss function below.

Assumption 1 (\mathcal{L} -Smooth Loss Function). The loss function is \mathcal{L} -smooth if its gradient $\nabla l : \mathbb{R}^d \rightarrow \mathbb{R}^d$ is \mathcal{L} -Lipschitz, i.e. there exists a constant $\mathcal{L} > 0$ such that

$$\forall \theta_1, \theta_2 \in \mathbb{R}^d, \quad \|\nabla l(\theta_2) - \nabla l(\theta_1)\|_2 \leq \mathcal{L} \|\theta_2 - \theta_1\|_2. \quad (5)$$

\mathcal{L} is also called the second-order Lipschitz constant. \mathcal{L} -smoothness is a recurring assumption in optimization theory [Nesterov et al., 2018, Bertsekas, 1997]. In practice, standard and adversarial losses are smooth for certain models [Li et al., 2017, Wu et al., 2020] and not others. Yet, in Section 6, our approach results in increased robustness for a variety of architectures. Leveraging this assumption, we state our main theorem below.

Theorem 1 (Sufficient Conditions for persistently exciting Model). If a model is trained by minimizing a \mathcal{L} -smooth loss (Assumption 1) via gradient descent with a learning rate schedule given by $(\eta^k)_{k \geq 1}$, then if $\eta^k < 1/\mathcal{L}$ for all k , the model will be persistently exciting (Problem Statement 1).

Proof Sketch: The complete proof is in Appendix A. First, utilizing Lemma 1, we prove that each trajectory in the family from Definition 3 is persistently exciting and GES. Second, we fit consecutive gradient descent updates to a persistently exciting trajectory from the desired family. To do so, we discretize the CT dynamics in time interval $[k, k+1]$ and substitute the gradient descent update step (3). Third, we leverage chosen trajectory characteristics (here, full rankness of $\Phi^k \Phi^{k\top}$) to find sufficient conditions under which our PoE condition from the previous step is satisfied.

Our three step proof provides a framework to obtain sufficient PoE conditions for any gradient update rule to track a desired family of persistently exciting dynamics. We postulate that this methodology can be adapted in future work for other gradient-based optimization methods like SGD, Adam [Kingma and Ba, 2014], and stochastic weight averaging (SWA) [Izmailov et al., 2018].

4.1 Connection to Convex Optimization.

In gradient descent on a \mathcal{L} -smooth and convex loss function, a learning rate choice of $\eta^k \leq \frac{1}{\mathcal{L}}$ guarantees monotonic progress to the minima [Nesterov et al., 2018]. Our similar result is expected because every persistently exciting trajectory, on which states converge exponentially fast to minima θ^* , is a convex shortcut from θ^k to θ^* through θ^{k+1} that may or may not lie on the loss surface. Our approach could be thought of as hopping along the points of intersection of convex shortcuts and the loss surface until convergence. This relationship both provides an interesting intuition for our approach and strengthens its validity.

4.2 Training with a Constant Learning Rate? Divide by two.

In gradient descent on any \mathcal{L} -smooth differentiable loss function with a fixed learning rate η , the algorithm converges to local minima if $\eta < \frac{2}{\mathcal{L}}$ [Bertsekas, 1997]. Thus, if a model is known to converge with a fixed learning rate via gradient descent, halving the learning rate should give rise to a persistently exciting model. Unfortunately the simplicity of dividing by two does not always work in practice because most modern training algorithms use SGD rather than gradient descent and learning schedules rather than a constant learning rate whereas this result is only valid for constant learning rate training. We discuss this gap in Section 4.4.

4.3 Playing it safe: The upper bound of $1/\mathcal{L}$ is conservative.

In the Proof for Theorem 1, we have a sufficient condition nested within another sufficient condition. The first, and less obvious, sufficient condition is the full rank nature of $\Phi^k \Phi^{k\top}$. This condition is sufficient but not *necessary* for the trajectory described by Equation (4) to be persistently exciting. Second, the upper bound $\eta^k < 1/\mathcal{L}$ is sufficient but not necessary for Equation (14) in Appendix A to be satisfied. With these two nested sufficient conditions, our upper bound $1/\mathcal{L}$ is conservative and values greater than it may also ensure PoE. In fact, we later conjecture that an upper bound of $2/\mathcal{L}$ may ensure PoE in Section 7. This is inspired by empirical successes in training a model either with a constant learning rate just below $2/\mathcal{L}$ in Section 5.2 or with a schedule starting just below $2/\mathcal{L}$ in standard/adversarial training in Sections 5.3 and 6.

4.4 Limitations of the Theory: Resolving the Gradient Descent-SGD Gap.

In practice, models are trained with with SGD and its accelerated variants [Nesterov et al., 2018] rather than gradient descent. Further, in SGD, a slowly-decaying learning rate schedule (such as a sequence obeying $\sum_k \eta^k = \infty$, $\sum_k \eta^{k^2} < \infty$ [Bottou et al., 2018]) is oftentimes necessary for training to converge in the first place. Thus to accommodate additional rules (apart from Theorem 1) on the learning rate schedule, we set the first learning rate as $\eta^1 = 1/\mathcal{L}_{\text{est}}$ (where \mathcal{L}_{est} is the estimated Lipschitz constant) and then scale every subsequent learning rate in the same proportion of the initial value as in the baseline schedule that is known to ensure convergence to some local optima. We discuss this trick in more detail in Section 5.1. Evaluations in Section 6 successfully demonstrate increased robustness in both standard and adversarially trained models using this initial learning rate modification and subsequent learning rate scaling.

5 Implementation

Following the derivation of our sufficient condition for PoE in Theorem 1, we elaborate on an implementation strategy in practical SGD based training such that we both satisfy the PoE condition and actually converge while training. The core part of our implementation strategy, an estimation algorithm for the Lipschitz constant \mathcal{L} based on extreme value theory [Wood and Zhang, 1996, Weng et al., 2018], is explained in this section. We also discuss some practical choices made regarding the learning rate schedule based on simple analysis experiments on the MNIST and CIFAR10 datasets. We conclude this section with a brief description of the added complexity of our approach.

5.1 Implementing PoE: How do we modify the learning rate schedule in practice?

First, we make an assumption that there exists a learning rate schedule (called *baseline schedule*) represented by $(\gamma^k)_{k \geq 1}$ with $\gamma^k \leq \gamma^1$ for all k , such that the model converges to some local optima.

Second, we set the initial learning rate η^1 to $1/\mathcal{L}_{\text{est}}$. We detail the algorithm for obtaining \mathcal{L}_{est} in Section 5.3. Our algorithm provides an estimate that is always larger than the true value [Wood and Zhang, 1996, Weng et al., 2018] ensuring that $\eta^1 = 1/\mathcal{L}_{\text{est}} < 1/\mathcal{L}_{\text{true}}$ which in turn means that η^1 satisfies Theorem 1. Using the baseline schedule as reference, we set $\eta^k = \eta^1 \gamma^k / \gamma^1$ for all $k \geq 2$. Each η^k , $k \geq 2$, now automatically satisfies the bound in Theorem 1. This means that we scaled the baseline schedule γ^k by the fraction η^1/γ^1 to get a schedule that satisfies Theorem 1 (and hence leads to a persistently exciting model) and also, because it follows a similar annealing cycle as the baseline schedule, converges in practice. We call this schedule the *persistently exciting schedule*.

Third, following the discussion in Section 4.3, we analyze another learning rate schedule called the *largest convergent schedule* where we set η^1 to $2/\mathcal{L}_{\text{est}}$ and scale the rest of the schedule like above with $\eta^k = \eta^1 \gamma^k / \gamma^1$ for all $k \geq 2$. This schedule also converges in practice and we later conjecture in Section 7 that it also leads to a persistently exciting model. An example of the above three learning schedules for three typical annealing strategies – step decay, exponential decay, and cosine annealing [Loshchilov and Hutter, 2016] is given in Figure 2.

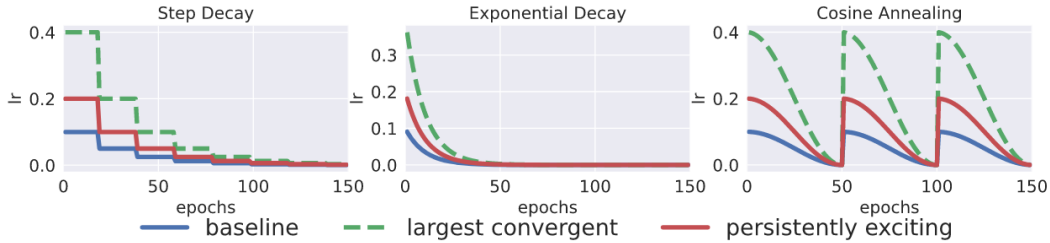


Figure 2: An e.g. of baseline ($\eta^1 = 0.1$), largest convergent ($\eta^1 = 2/\mathcal{L}$) and persistently exciting ($\eta^1 = 1/\mathcal{L}$) learning rate (lr) schedules. Here, $\mathcal{L} = 5$ and the latter two start above baseline. Another e.g. with $\mathcal{L} = 15$, where persistently exciting schedule starts below baseline, is in Appendix D.

5.2 Practical Choices: Working at the Edge with $1/\mathcal{L}_{\text{est}}$ and $2/\mathcal{L}_{\text{est}}$

Our choice of initial learning rate $\eta^1 = 1/\mathcal{L}_{\text{est}}$ which is close to the upper bound in Theorem 1 stems from an experimental analysis of adversarial accuracy versus learning rate. We trained a LeNet5 model [LeCun et al., 1998] with various constant learning rates for 10 epochs on the MNIST dataset.

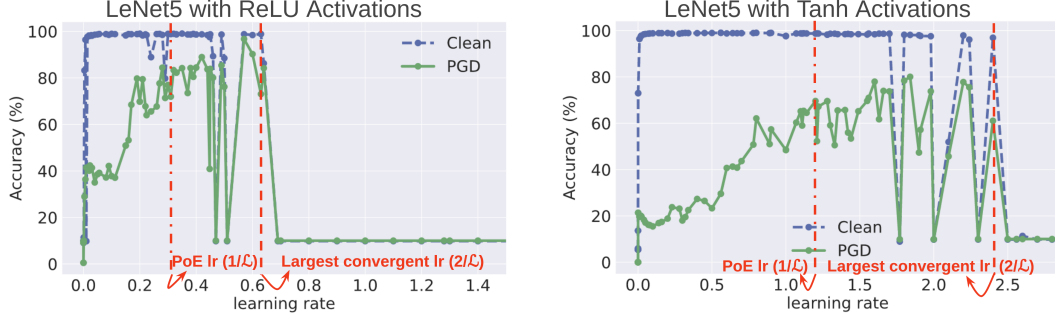


Figure 3: Accuracy on Clean and PGD attacked MNIST validation set for LeNet5 models (with ReLU [left] and Tanh [right] activations) vs constant learning rate (lr) used in training. The largest convergent lr ($2/\mathcal{L}_{\text{est}}$) and the PoE lr ($1/\mathcal{L}_{\text{est}}$) have higher PGD accuracy than baseline lr (0.1).

Each trained model is evaluated against a 40-step PGD attack with perturbation budget of $\epsilon = 0.3$. This leads to the plots of clean and adversarial accuracy in Figure 3. The Figure on the left is for a LeNet5 model with ReLU activations and the one on the right is for one with Tanh activations.

Both the left and right plots in Figure 3 indicate that adversarial accuracy peaks at or just to the left of the largest learning rate at which the model converges to a local optima (*i.e.* when Clean accuracy is close to 100 %). Since we are training with a constant learning rate, the value of largest convergent learning rate is theoretically given by $2/\mathcal{L}$ [Bertsekas, 1997]. For this reason, we choose to investigate a schedule with an initial learning rate at $2/\mathcal{L}_{\text{est}}$. Also, at half this point (our upper bound of $1/\mathcal{L}$), we notice adversarial accuracy is still high. But moving to the left of said point, we notice a drop in adversarial accuracy. This drop can be explained by the ill-conditioning of $\|\nabla l(\theta^k)\|_2/\|\theta^k - \theta^*\|$ term in inequality (12) in our proof in Appendix A. This happens because the denominator, which is the L2 distance between the model weights and true weights, is forced to be a small value for small learning rates. Moreover, since it is hard to predict the exact start point of the decay in adversarial accuracy, we choose to remain closer to the upper bound and work with $1/\mathcal{L}_{\text{est}}$ and $2/\mathcal{L}_{\text{est}}$.

5.3 Estimation of Certified Lipschitz Constant \mathcal{L} via Extreme Value Theory

Inspired by existing literature [Wood and Zhang, 1996, Weng et al., 2018], we estimate \mathcal{L} with the three following steps, which we believe detail the first application of extreme value theory to the loss gradient’s Lipschitz constant estimation (rather than the well-studied network Lipschitz constant).

First, collect average loss gradient and model parameters after each epoch in baseline training (*i.e.* with the baseline schedule). They are vectors denoted by $(\nabla l(\theta^i), \theta^i)_{1, \dots, N_{\text{epochs}}}$.

Second, estimate a Lipschitz constant. To start with, compute $N/2$ slopes by sampling N points and finding the slopes between consecutive pairs as $s_i = \frac{\|\nabla l(\theta^{i+1}) - \nabla l(\theta^i)\|_2}{\|\theta^{i+1} - \theta^i\|_2}$, $i = 1, 3, 5, \dots, N$. Next, we compute the maximum of these $N/2$ slopes as, $l = \max\{s_1, s_3, s_5, \dots, s_N\}$. We repeat this process M times to obtain $\{l_1, \dots, l_M\}$. Now, based on the Fisher–Tippett–Gnedenko theorem [De Haan and Ferreira, 2007], we fit a three parameter (shape, location, scale) reverse Weibull distribution to these M points given an initial value for the shape parameter (shape_0). The fitted scale parameter is the desired estimate of Lipschitz constant.

Third, certify the estimated Lipschitz constant. We run a Kolmogorov–Smirnov (K-S) test to test the null hypothesis that our samples $\{l_1, \dots, l_M\}$ are drawn from a reverse Weibull distribution with the fitted parameters. We repeat Step (2) for different initial shape values and repeatedly perform the K-S test. This gives us various p-values and we choose the Lipschitz constant (*i.e.*, scale parameter) corresponding to the highest p-value. However, a question still remains- how are the hyper-parameters (M, N) tuned? To answer this, we propose the following heuristic that works well in practice.

A heuristic for hyper-parameter (M, N) tuning. Repeat Steps (2) and (3) for different M and N . Assume a mid-to-large significance value (*e.g.*, $\alpha = 0.4$ to 0.6). Among various (M, N) choices, choose the Lipschitz constant from the case when atleast one p-value is larger than α and atleast one p-value is less than α . A more detailed explanation of all of the above can be found in Appendix B.

Following the above, we estimate Lipschitz constant for ResNet20 standard training with $\alpha = 0.55$. We get $\mathcal{L}_{\text{est}} = 3.5258$ for $(M, N) = (200, 100)$. Plotting clean and PGD accuracy in Figure 4, we observe in Figure 4b that models trained with the persistently exciting and largest convergent

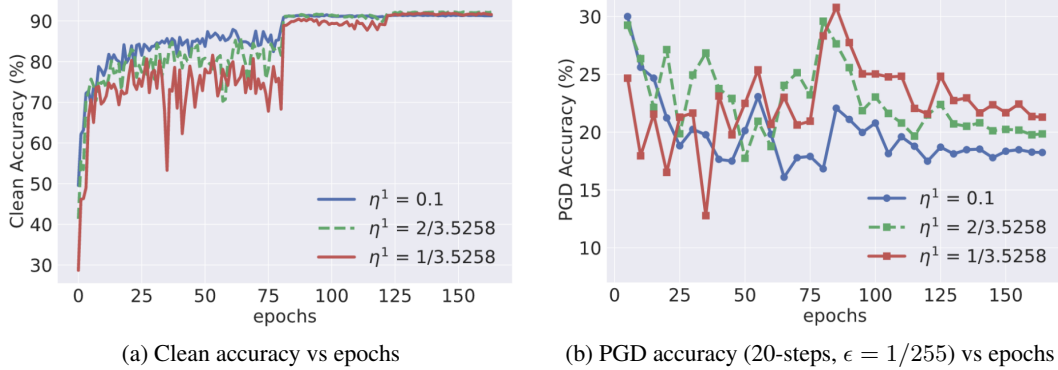


Figure 4: Lipschitz constant \mathcal{L}_{est} estimated for ResNet20 standard training is 3.5258. Training with persistently exciting schedule ($\eta^1 = 1/\mathcal{L}_{\text{est}}$) and largest convergent schedule ($\eta^1 = 2/\mathcal{L}_{\text{est}}$) results in consistent PGD accuracy increase while matching clean accuracy of baseline (see epochs 80-164).

schedules have consistently better adversarial accuracy (see epochs 80-164) than the baseline model while matching its clean accuracy in Figure 4a (More detailed analysis in Appendix B).

5.4 Linear Increase in Time Complexity

Our primary increase in training time is a consequence of having to train a baseline model and then another model with a persistently exciting schedule. This results in a $2\times$ increase in time. We hope future work can help boost performance (for *e.g.*, by adapting learning rates online to satisfy PoE conditions). A complete time complexity and memory overhead analysis is given in Appendix B.

6 Results: PoE is a ‘Force-Multiplier’ for Robustness

Following the implementation details in Section 5.1, we perform both standard training and adversarial training with a baseline schedule, persistently exciting schedule and largest convergent schedule. The clean and adversarial accuracy results for standard training is presented in Table 1; for adversarial training in Table 2. For standard training (*i.e.* minimizing cross-entropy loss on natural images), we analyze LeNet5, ResNet 20, 50, 110 [He et al., 2016], and DenseNet 40 [Huang et al., 2017] on CIFAR10 dataset; and ResNet 50, 110 and DenseNet 40 on CIFAR100 dataset. The hyperparameters and training details for standard SGD training are given in Appendix D. The values of M , N , \mathcal{L}_{est} as well as η^1 and the learning rate schedule for each of the 3 methods- baseline, persistently exciting, and largest convergent are also given in Appendix D. We evaluate each CIFAR10 and CIFAR100 model after training completes against a 20-step PGD adversary with $\epsilon = 1/255$, step-size of $0.1/255$, and no random restarts. The adversary is a PGD attack (albeit, on the slightly weaker side in terms of perturbation budget) because demonstrating robustness against PGD guarantees robustness to a wide range of first-order adversaries [Madry et al., 2017]. We also include the results of LeNet5 model on MNIST dataset from Section 5.2 in Table 1. Please note that the MNIST model is evaluated against a stronger 40-step PGD adversary with $\epsilon = 0.3$, step-size of 0.01, and with random restarts.

For adversarial training (on CIFAR10), we train a ResNet-50 in a PGD-AT framework [Madry et al., 2017]; WideResNet (WRN) 34-10 [Zagoruyko and Komodakis, 2016] in a TRADES framework [Zhang et al., 2019]; WRN 28-10 in a RST framework [Carmon et al., 2019]; and WRN 34-15 in a Wide-RST framework [Wu et al., 2021]. All four frameworks are detailed in Appendix C. The latter two utilize 500K additional unlabelled images from the Tiny Images dataset [Torralba et al., 2008]. The hyperparameters and training details for adversarial training are given in Appendix D. The values of M , N , \mathcal{L}_{est} as well as η^1 and the learning rate schedule for each of the 3 methods- baseline, persistently exciting, and largest convergent in all frameworks are also given in Appendix D. All code bases referenced are in Appendix D. We evaluate each model on Autoattack with $\epsilon = 8/255$. Autoattack is used as it provides an almost-hyperparameter free, unified benchmark to compare various adversarially robust models against both white and black-box attacks.

Discussion of results. In Table 1, we show a clear improvement in PGD accuracy over baseline with both the largest convergent and persistently exciting schedules. This demonstrates that our approach is promising. In Table 2, we have small but consistent (across AT frameworks and models) improvements in AutoAttack accuracy with largest convergent schedule taking the lead closely followed by persistently exciting schedule. We assert that the results in Table 2 are noteworthy since

Dataset	Model	baseline η^1		Largest Convergent $\eta^1 = 2/\mathcal{L}$ (Ours)		Persistently Exciting $\eta^1 = 1/\mathcal{L}$ (Ours)	
		Clean	PGD	Clean	PGD	Clean	PGD
MNIST	LeNet 5 (relu)	99.0	30.0*	99.0	73.1*	99.0	72.0*
	LeNet 5 (tanh)	99.0	16.1*	97.0	<u>61.1*</u>	98.8	70.0*
CIFAR 10	LeNet 5 (relu)	57.27	39.21	59.93	43.7	54.39	42.63
	LeNet 5 (tanh)	53.18	40.82	54.37	41.16	55.95	43.84
	ResNet 20	91.29	18.24	92.18	<u>19.85</u>	91.57	21.30
	ResNet 50	93.16	21.66	93.41	25.91	93.25	25.28
	ResNet 110	93.38	29.60	93.58	43.87	93.38	<u>30.1</u>
	DenseNet 40	93.30	8.80	93.43	<u>8.80</u>	93.0	10.70
CIFAR 100	ResNet 50	70.74	5.57	70.94	<u>5.69</u>	70.15	6.2
	ResNet 110	71.63	10.04	71.92	10.23	71.13	<u>7.98</u>
	DenseNet 40	71.64	1.38	69.9	2.10	70.22	<u>1.57</u>

Table 1: Standard trained models evaluated against 20-step PGD adversary with perturbation budget $\epsilon = 1/255$. The number with the bold face and the underline denote the best and the second best result, respectively. (* marked points are evaluated on a stronger 40-step PGD attack with $\epsilon = 0.3$.)

Approach	Model	Current SOTA		Largest Convergent $\eta^1 = 2/\mathcal{L}$ (Ours)		Persistently Exciting $\eta^1 = 1/\mathcal{L}$ (Ours)	
		Clean	Autoattack	Clean	Autoattack	Clean	Autoattack
PGD-AT	ResNet-50	86.05	42.72	86.46	43.00	85.73	42.84
TRADES	WRN-34-10	84.40	52.17	83.24	52.32	84.36	<u>52.19</u>
RST*	WRN-28-10	89.5	59.40	89.46	59.66	89.68	<u>59.46</u>
Wide-RST*	WRN-34-15	86.51	<u>60.28</u>	86.53	60.41	85.97	<u>59.87</u>

Table 2: Adversarial trained models evaluation against AutoattackAttack on CIFAR10 with perturbation budget $\epsilon = 8/255$. The number with the bold face and the underline denote the best and the second best result, respectively. Astrisk (*) indicates extra unlabeled data used.

improvements of 0.04 are considered significant in the AutoAttack benchmark. Our approach is theoretically motivated, demonstrates universal improvements in adversarial accuracy and is easy to implement. For these reasons, we argue that PoE is a clear ‘force-multiplier’ for robustness and a crucial ‘tool’ for future progress in robustness.

Discussion on other RobustBench competitors. We note that recent work [Gowal et al., 2020, Rebuffi et al., 2021] edges out Wide-RST for first place on the AutoAttack benchmark but because this work does not make its code base (for training their models) publicly available, we are unable to include it in our results. Nevertheless, our theoretical framework and empirical successes guarantee that applying our approach to this variant will improve its robustness.

Potential negative societal impacts. Our approach improves robustness of models universally but requires careful consideration of all possible attack surfaces (and guarantees on robustness to the same) when facing real-world adversaries in safety-critical systems to avoid fatal consequences. When combined with existing development techniques, our approach may decrease the likelihood of bad consequences, but will never increase it.

7 Conclusions and Future Work

In this paper, we prove a sufficient condition for PoE of gradient descent in terms of an upper bound on learning rates given by $1/\mathcal{L}$ (where \mathcal{L} is the Lipschitz constant of gradient of loss). We scale a baseline learning rate schedule setting the starting value just below $1/\mathcal{L}$ to satisfy our PoE condition. We propose an efficient algorithm to estimate this Lipschitz constant (and certify it) with extreme value theory. Applying our scaled learning rate schedule results in improved robustness in both standard and adversarial training, demonstrating its effectiveness as a ‘force-multiplier’.

We also conjecture based on experimental results (Section 6) and the conservative nature of our upper bound (Section 4.3) that a learning rate schedule starting just below $2/\mathcal{L}$ is persistently exciting. Finding a reference family of dynamics to prove the same is an open problem. Other open problems include identifying PoE conditions for SGD, Adam, SWA and their variants as well as applying PoE to unsupervised and semi-supervised domains.

Acknowledgments and Disclosure of Funding

References

- K.-J. Åström and B. Torsten. Numerical identification of linear dynamic systems from normal operating records. *IFAC Proceedings Volumes*, 2(2):96–111, 1965.
- A. Athalye, N. Carlini, and D. Wagner. Obfuscated gradients give a false sense of security: Circumventing defenses to adversarial examples. In *International Conference on Machine Learning*, pages 274–283. PMLR, 2018.
- D. P. Bertsekas. Nonlinear programming. *Journal of the Operational Research Society*, 48(3): 334–334, 1997.
- B. Biggio, I. Corona, D. Maiorca, B. Nelson, N. Šrndić, P. Laskov, G. Giacinto, and F. Roli. Evasion attacks against machine learning at test time. In *Joint European conference on machine learning and knowledge discovery in databases*, pages 387–402. Springer, 2013.
- L. Bottou, F. E. Curtis, and J. Nocedal. Optimization methods for large-scale machine learning. *Siam Review*, 60(2):223–311, 2018.
- N. Carlini and D. Wagner. Adversarial examples are not easily detected: Bypassing ten detection methods. In *Proceedings of the 10th ACM Workshop on Artificial Intelligence and Security*, pages 3–14, 2017.
- Y. Carmon, A. Raghunathan, L. Schmidt, P. Liang, and J. C. Duchi. Unlabeled data improves adversarial robustness. *arXiv preprint arXiv:1905.13736*, 2019.
- P. Chaudhari, A. Choromanska, S. Soatto, Y. LeCun, C. Baldassi, C. Borgs, J. Chayes, L. Sagun, and R. Zecchina. Entropy-sgd: Biasing gradient descent into wide valleys. *Journal of Statistical Mechanics: Theory and Experiment*, 2019(12):124018, 2019.
- T. Chen, S. Liu, S. Chang, Y. Cheng, L. Amini, and Z. Wang. Adversarial robustness: From self-supervised pre-training to fine-tuning. In *Proceedings of the IEEE/CVF Conference on Computer Vision and Pattern Recognition*, pages 699–708, 2020.
- T. Chen, Z. Zhang, S. Liu, S. Chang, and Z. Wang. Robust overfitting may be mitigated by properly learned smoothening. In *International Conference on Learning Representations*, volume 1, 2021.
- J. Cohen, E. Rosenfeld, and Z. Kolter. Certified adversarial robustness via randomized smoothening. In *International Conference on Machine Learning*, pages 1310–1320. PMLR, 2019.
- F. Croce and M. Hein. Reliable evaluation of adversarial robustness with an ensemble of diverse parameter-free attacks. In *ICML*, 2020.
- L. De Haan and A. Ferreira. *Extreme value theory: an introduction*. Springer Science & Business Media, 2007.
- G. W. Ding, L. Wang, and X. Jin. AdverTorch v0.1: An adversarial robustness toolbox based on pytorch. *arXiv preprint arXiv:1902.07623*, 2019.
- I. J. Goodfellow, J. Shlens, and C. Szegedy. Explaining and harnessing adversarial examples. *arXiv preprint arXiv:1412.6572*, 2014.
- D. Gorinevsky. On the persistency of excitation in radial basis function network identification of nonlinear systems. *IEEE Transactions on Neural Networks*, 6(5):1237–1244, 1995. doi: 10.1109/72.410365.
- S. Gowal, C. Qin, J. Uesato, T. Mann, and P. Kohli. Uncovering the limits of adversarial training against norm-bounded adversarial examples. *arXiv preprint arXiv:2010.03593*, 2020.
- K. He, X. Zhang, S. Ren, and J. Sun. Deep residual learning for image recognition. In *Proceedings of the IEEE conference on computer vision and pattern recognition*, pages 770–778, 2016.
- D. Hendrycks, K. Lee, and M. Mazeika. Using pre-training can improve model robustness and uncertainty. In *International Conference on Machine Learning*, pages 2712–2721. PMLR, 2019.
- G. Huang, Z. Liu, L. Van Der Maaten, and K. Q. Weinberger. Densely connected convolutional networks. In *Proceedings of the IEEE conference on computer vision and pattern recognition*, pages 4700–4708, 2017.
- P. A. Ioannou and J. Sun. *Robust adaptive control*. Courier Corporation, 2012.

- P. Izmailov, D. Podoprikin, T. Garipov, D. Vetrov, and A. G. Wilson. Averaging weights leads to wider optima and better generalization. *arXiv preprint arXiv:1803.05407*, 2018.
- D. P. Kingma and J. Ba. Adam: A method for stochastic optimization. *arXiv preprint arXiv:1412.6980*, 2014.
- A. Krizhevsky, G. Hinton, et al. Learning multiple layers of features from tiny images. 2009.
- A. Kurdila, F. J. Narcowich, and J. D. Ward. Persistency of excitation in identification using radial basis function approximants. *SIAM journal on control and optimization*, 33(2):625–642, 1995.
- Y. LeCun. The mnist database of handwritten digits. <http://yann.lecun.com/exdb/mnist/>, 1998.
- Y. LeCun, L. Bottou, Y. Bengio, and P. Haffner. Gradient-based learning applied to document recognition. *Proceedings of the IEEE*, 86(11):2278–2324, 1998.
- M. Lecuyer, V. Atlidakis, R. Geambasu, D. Hsu, and S. Jana. Certified robustness to adversarial examples with differential privacy. In *2019 IEEE Symposium on Security and Privacy (SP)*, pages 656–672. IEEE, 2019.
- B. Li, C. Chen, W. Wang, and L. Carin. Certified adversarial robustness with additive noise. *arXiv preprint arXiv:1809.03113*, 2018.
- H. Li, Z. Xu, G. Taylor, C. Studer, and T. Goldstein. Visualizing the loss landscape of neural nets. *arXiv preprint arXiv:1712.09913*, 2017.
- I. Loshchilov and F. Hutter. Sgdr: Stochastic gradient descent with warm restarts. *arXiv preprint arXiv:1608.03983*, 2016.
- S. Lu and T. Basar. Robust nonlinear system identification using neural-network models. *IEEE Transactions on Neural networks*, 9(3):407–429, 1998.
- A. Madry, A. Makelov, L. Schmidt, D. Tsipras, and A. Vladu. Towards deep learning models resistant to adversarial attacks. *arXiv preprint arXiv:1706.06083*, 2017.
- K. Nar and S. S. Sastry. Persistency of excitation for robustness of neural networks. *arXiv preprint arXiv:1911.01043*, 2019.
- K. S. Narendra and A. M. Annaswamy. *Stable adaptive systems*. Courier Corporation, 2012.
- Y. Nesterov et al. *Lectures on convex optimization*, volume 137. Springer, 2018.
- T. Pang, X. Yang, Y. Dong, H. Su, and J. Zhu. Bag of tricks for adversarial training. *arXiv preprint arXiv:2010.00467*, 2020a.
- T. Pang, X. Yang, Y. Dong, K. Xu, J. Zhu, and H. Su. Boosting adversarial training with hypersphere embedding. *arXiv preprint arXiv:2002.08619*, 2020b.
- M. M. Polycarpou and P. A. Ioannou. *Identification and control of nonlinear systems using neural network models: Design and stability analysis*. Citeseer, 1991.
- S.-A. Rebuffi, S. Gowal, D. A. Calian, F. Stimberg, O. Wiles, and T. Mann. Fixing data augmentation to improve adversarial robustness. *arXiv preprint arXiv:2103.01946*, 2021.
- L. Rice, E. Wong, and Z. Kolter. Overfitting in adversarially robust deep learning. In *International Conference on Machine Learning*, pages 8093–8104. PMLR, 2020.
- S. Sastry and M. Bodson. *Adaptive control: stability, convergence and robustness*. Courier Corporation, 2011.
- V. Sehwag, S. Wang, P. Mittal, and S. Jana. Hydra: Pruning adversarially robust neural networks. *Advances in Neural Information Processing Systems (NeurIPS)*, 7, 2020.
- V. Sehwag, S. Mahloujifar, T. Handina, S. Dai, C. Xiang, M. Chiang, and P. Mittal. Improving adversarial robustness using proxy distributions. *arXiv preprint arXiv:2104.09425*, 2021.
- C. Sitawarin, S. Chakraborty, and D. Wagner. Improving adversarial robustness through progressive hardening. *arXiv preprint arXiv:2003.09347*, 2020.
- S. Sukumar and M. R. Akella. Persistence filters for estimation: Applications to control in shared-sensing reversible transducer systems. *Journal of dynamic systems, measurement, and control*, 134(4), 2012.
- C. Szegedy, W. Zaremba, I. Sutskever, J. Bruna, D. Erhan, I. Goodfellow, and R. Fergus. Intriguing properties of neural networks. *arXiv preprint arXiv:1312.6199*, 2013.

- A. Torralba, R. Fergus, and W. T. Freeman. 80 million tiny images: A large data set for nonparametric object and scene recognition. *IEEE transactions on pattern analysis and machine intelligence*, 30(11):1958–1970, 2008.
- J. Uesato, J.-B. Alayrac, P.-S. Huang, R. Stanforth, A. Fawzi, and P. Kohli. Are labels required for improving adversarial robustness? *arXiv preprint arXiv:1905.13725*, 2019.
- Y. Wang, D. Zou, J. Yi, J. Bailey, X. Ma, and Q. Gu. Improving adversarial robustness requires revisiting misclassified examples. In *International Conference on Learning Representations*, 2019.
- T.-W. Weng, H. Zhang, P.-Y. Chen, J. Yi, D. Su, Y. Gao, C.-J. Hsieh, and L. Daniel. Evaluating the robustness of neural networks: An extreme value theory approach. *arXiv preprint arXiv:1801.10578*, 2018.
- G. Wood and B. Zhang. Estimation of the lipschitz constant of a function. *Journal of Global Optimization*, 8(1):91–103, 1996.
- B. Wu, J. Chen, D. Cai, X. He, and Q. Gu. Do wider neural networks really help adversarial robustness?, 2021.
- D. Wu, S.-T. Xia, and Y. Wang. Adversarial weight perturbation helps robust generalization. *Advances in Neural Information Processing Systems*, 33, 2020.
- S. Zagoruyko and N. Komodakis. Wide residual networks. *arXiv preprint arXiv:1605.07146*, 2016.
- H. Zhang, Y. Yu, J. Jiao, E. Xing, L. El Ghaoui, and M. Jordan. Theoretically principled trade-off between robustness and accuracy. In *International Conference on Machine Learning*, pages 7472–7482. PMLR, 2019.
- J. Zhang, J. Zhu, G. Niu, B. Han, M. Sugiyama, and M. Kankanhalli. Geometry-aware instance-reweighted adversarial training. *arXiv preprint arXiv:2010.01736*, 2020.

Appendix

A Proof of Theorem 1

The proof of Theorem 1 is detailed below.

Proof. First, let's prove that each trajectory in the family from Definition 3 is persistently exciting and GES. (GES implies that the states on trajectories given by (4) are guaranteed to converge exponentially fast to the equilibrium at the true parameters). We can prove that $\Phi(t)$ is persistently exciting. Let $k = \lfloor t \rfloor$, and choose $0 < T_0 \leq \lceil t \rceil - t$ such that

$$\int_t^{t+T_0} \Phi(s)\Phi(s)^\top ds = \Phi^k \Phi^k{}^\top T_0 \quad (6)$$

Since full rank matrix (Definition 3) given by $\Phi^k \Phi^k{}^\top$ is naturally symmetric and positive definite, all of its eigenvalues are strictly positive. Hence, we have,

$$0 < \lambda_{\min} T_0 \mathbf{I} \leq \Phi^k \Phi^k{}^\top T_0 \leq \lambda_{\max} T_0 \mathbf{I} \quad (7)$$

where $\lambda_{\min}, \lambda_{\max} > 0$ are the minimum and maximum eigenvalues of symmetric, positive definite $\Phi^k \Phi^k{}^\top$. Thus, via Definition 1, $\Phi(t)$ is persistently exciting. Also, $\Phi(t)$ is given to be piecewise continuous. Therefore, we have GES as a consequence of Lemma 1.

Second, let's fit consecutive gradient descent updates to a persistently exciting trajectory from the desired family. For θ^{k+1} to lie on the system in Definition 3, set $\Gamma(k+1) = \theta^{k+1}$. Next, discretizing the CT dynamics in time period $[k, k+1]$, we get,

$$\theta^{k+1} - \theta^* = e^{-\Phi^k \Phi^k{}^\top} (\theta^k - \theta^*) \quad (8)$$

$$\implies \theta^{k+1} - \theta^k = -(\mathbf{I} - e^{-\Phi^k \Phi^k{}^\top}) (\theta^k - \theta^*) \quad (9)$$

Substituting the gradient descent update step (3), we have,

$$-\eta^k \nabla l(\theta^k) = -(\mathbf{I} - e^{-\Phi^k \Phi^k{}^\top}) (\theta^k - \theta^*) \quad (10)$$

$$\implies \frac{\eta^k \|\nabla l(\theta^k)\|_2}{\|\theta^k - \theta^*\|_2} \leq \|(\mathbf{I} - e^{-\Phi^k \Phi^k{}^\top})\|_2 \quad (11)$$

$$= \max |\text{eig}(\mathbf{I} - e^{-\Phi^k \Phi^k{}^\top})| \quad (12)$$

Therefore, if (12) is satisfied, then, for any two consecutive updates of gradient descent given by θ^k and θ^{k+1} , we will have ensured that $\Gamma(k) = \theta^k$ and $\Gamma(k+1) = \theta^{k+1}$. This means that satisfying (12) is equivalent to fitting consecutive gradient descent updates on the persistently exciting trajectory. Thus, we can now move to the third step as given below.

Third, let's find sufficient conditions under which our PoE condition (Inequality (12)) is satisfied. Since $\Phi^k \Phi^k{}^\top$ is symmetric and positive definite, we observe that it can be written as UDU^\top where D is a positive definite diagonal matrix. The eigenvalues of $(\mathbf{I} - e^{-\Phi^k \Phi^k{}^\top})$ are given by the elements of the diagonal matrix $(\mathbf{I} - e^{-D})$, all of whom lie in the interval $(0, 1)$. Hence, substituting $\max |\text{eig}(\mathbf{I} - e^{-\Phi^k \Phi^k{}^\top})| < 1$ in (12), we obtain the following requirement for a persistently exciting model,

$$\frac{\|\nabla l(\theta^k)\|_2}{\|\theta^k - \theta^*\|_2} < \frac{1}{\eta^k} \implies \frac{\|\nabla l(\theta^k) - 0\|_2}{\|\theta^k - \theta^*\|_2} < \frac{1}{\eta^k} \quad (13)$$

$$\implies \frac{\|\nabla l(\theta^k) - \nabla l(\theta^*)\|_2}{\|\theta^k - \theta^*\|_2} < \frac{1}{\eta^k} \quad (\text{since } \nabla l(\theta^*) = 0) \quad (14)$$

which is sufficiently satisfied if $\mathcal{L} < \frac{1}{\eta^k}$ or equivalently, $\eta^k < \frac{1}{\mathcal{L}}$ for all k . \square

Algorithm 1: Estimation of Certified Lipschitz Constant**Input** : All saved gradients and parameters $(\nabla l(\theta^i), \theta^i)$, M , N , initial shape choices**Output** : \mathcal{L}_{est} **for** shape_0 in initial shape choices **do****for** $j = 1, \dots, M$ **do**Sample N points: $(\nabla l(\theta^i), \theta^i)_{i=1, \dots, N}$.Compute $N/2$ slopes between consecutive pairs of points:

$$s_i = \frac{\|\nabla l(\theta^{i+1}) - \nabla l(\theta^i)\|_2}{\|\theta^{i+1} - \theta^i\|_2}, \quad i = 1, 3, 5, \dots, N.$$

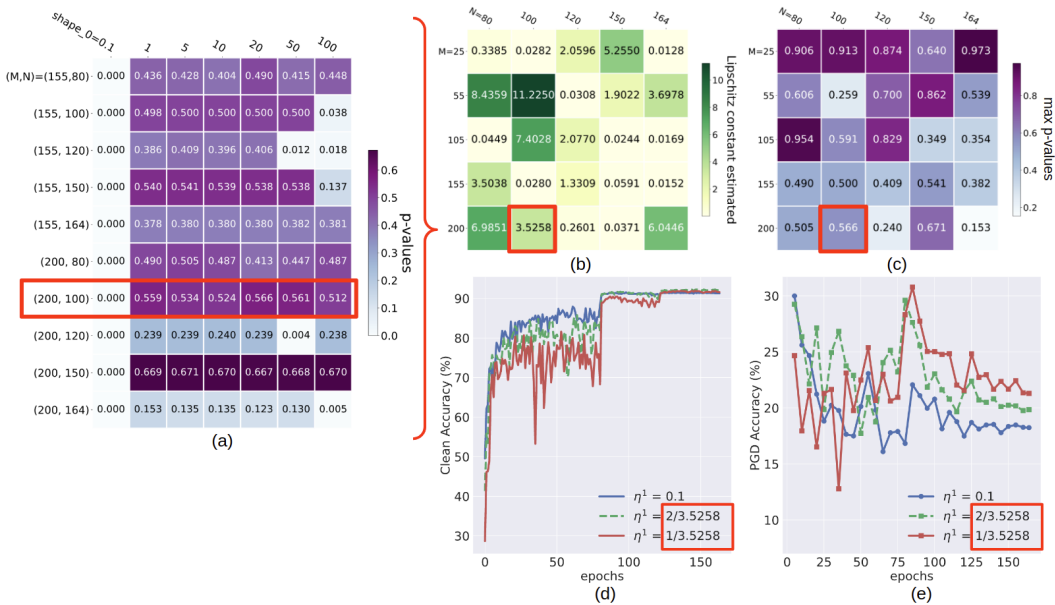
Compute maximum of the $N/2$ slopes: $l_j = \max\{s_1, s_3, s_5, \dots, s_N\}$.**end for**(shape, location, scale) \leftarrow Fit three parameter reverse Weibull distribution to $\{l_1, \dots, l_M\}$ given initial shape value = shape_0 .p-value \leftarrow Kolmogorov-Smirnov goodness-of-fit test.**end for****return** scale corresponding to largest p-value

Figure 5: Estimating \mathcal{L} for ResNet-20 model in standard classifier training using initial shape choices = $\{0.1, 1, 5, 10, 20, 50, 100\}$, $M \in \{25, 55, 105, 155, 200\}$, $N \in \{80, 100, 120, 150, 164\}$, and significance value $\alpha = 0.55$. Here, (a) shows a heat map of p-values for some (M, N) tuples vs shape_0 values; (b) shows Lipschitz constant estimates for all M, N values in a heat map; (c) depicts their corresponding max p-values (also in a heat map); (d) shows Clean accuracy vs epochs for baseline training, persistently exciting training with $\eta^1 = 1/3.5258$, and largest convergent training with $\eta^1 = 2/3.5258$; (e) compares the same three and shows adversarial accuracy vs epochs (against 20-step PGD with $\epsilon = 1/255$).

B Estimation of Certified Lipschitz Constant \mathcal{L} via Extreme Value Theory

Inspired by existing literature [Wood and Zhang, 1996, De Haan and Ferreira, 2007, Weng et al., 2018], we estimate \mathcal{L} with the three following steps. We believe that the following steps detail the first utilization of extreme value theory for the estimation of Lipschitz constant of the loss gradient (rather than well-studied estimation of Lipschitz constant of the neural network).

First, collect average loss gradient and model parameters after each epoch in baseline training (*i.e.* with the baseline schedule). They are vectors denoted by $(\nabla l(\theta^i), \theta^i)_{1, \dots, N_{\text{epochs}}}$.

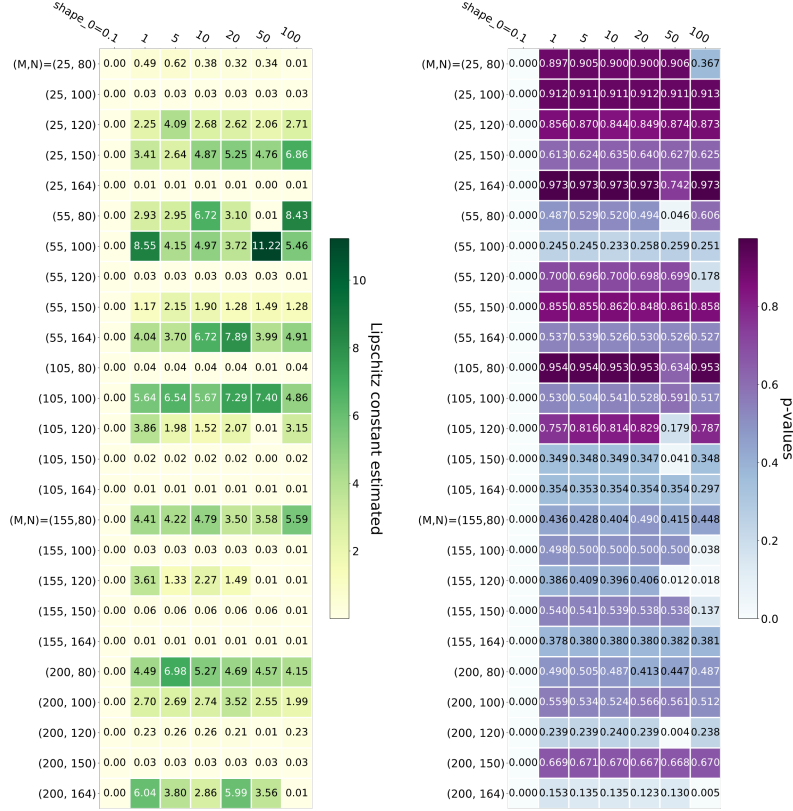


Figure 6: [LEFT] heat map of Lipschitz constants estimated (*i.e.* fitted scale parameter) for various (M, N) tuples vs various initial shape parameters. [RIGHT] heat map of corresponding p-values for various (M, N) tuples vs various initial shape parameters.

Second, estimate a Lipschitz constant. To start with, compute $N/2$ slopes by sampling N points and finding the slope between consecutive pairs as

$$s_i = \frac{\|\nabla l(\theta^{i+1}) - \nabla l(\theta^i)\|_2}{\|\theta^{i+1} - \theta^i\|_2}, \quad i = 1, 3, 5, \dots, N. \quad (15)$$

By using consecutive pairs for slope computation, we avoid using the same point more than once. Hence, we satisfy extreme value theory's integral assumption on independence of samples [Wood and Zhang, 1996, De Haan and Ferreira, 2007]. Next, we compute the maximum of these $N/2$ slopes as, $l = \max\{s_1, s_3, s_5, \dots, s_N\}$. We repeat this process M times to obtain $\{l_1, \dots, l_M\}$. Now, based on the Fisher–Tippett–Gnedenko theorem [De Haan and Ferreira, 2007] and assuming the Gnedenko condition, we fit a three parameter (shape, location, scale) reverse Weibull distribution to these M points. The three parameters are obtained via a maximum likelihood fit given an initial value for the shape parameter (that we denote by shape_0). The fitted scale parameter is the desired estimate of Lipschitz constant.

Third, certify the estimated Lipschitz constant. We run a Kolmogorov–Smirnov (K-S) test to test the null hypothesis that our samples $\{l_1, \dots, l_M\}$ are drawn from a reverse Weibull distribution with the fitted parameters. We repeat Step (2) for different initial shape values and repeatedly perform the K-S test. This gives us various p-values (one for each shape_0). Finally, we choose the Lipschitz constant (*i.e.*, scale parameter) corresponding to the highest p-value. The second and third Steps are outlined in Algorithm 1. Even with the above three steps, a question still remains- how are the hyper-parameters (M, N) tuned? To answer the same, we propose the following heuristic that works well in practice.

A heuristic for hyper-parameter (M, N) tuning. Repeat Steps (2) and (3) for different values of M and N . Assume a mid-to-large significance value (such as $\alpha = 0.4$ to $\alpha = 0.6$). Among the various

(M, N) choices, choose the Lipschitz constant from the case when atleast one p-value is larger than α and atleast one p-value is less than α .

This heuristic is depicted in Figure 5 for a ResNet-20 model [He et al., 2016] and a significance value of $\alpha = 0.55$. The row corresponding to $(M, N) = (200, 100)$ in Figure 5(a) is the only one that has both, p-values larger & lesser than α (satisfying our heuristic) and the largest of these corresponds to a Lipschitz constant of 3.5258 (see red box on Figure 5(b)). Thus, our estimated Lipschitz constant is $\mathcal{L}_{\text{est}} = 3.5258$. Please find the complete extended version of Figure 5(a), *i.e.* a complete heat map of all (M,N) tuples vs p-values in Figure 6 below.

Next, we perform standard classifier training (from scratch) for ResNet-20 on CIFAR10 by minimizing cross-entropy loss for 164 epochs with a baseline schedule starting at 0.1. The learning rate is divided by 10 at epochs 81 and 122. We compare the aforementioned baseline training with persistently exciting training which starts at a learning rate of $1/3.5258$ and follows the same learning rate decay at the same epochs. We also train with the largest convergent schedule starting at $2/3.5258$ (again, with the same decay at the same epochs). Plotting the variation of clean and adversarial accuracy (against 20-step PGD with $\epsilon = 1/255$ and step-size $0.1/255$) in Figures 5(d) and 5(e) respectively, we observe, in Figure 5(e), that after an initial chaotic period (see epochs 1-80), the model trained with the initial persistently exciting learning rate of $1/3.5258$ (or that trained with $2/3.5258$) has a consistently better adversarial accuracy (see epochs 80-164) than the baseline model while matching its clean accuracy in Figure 5(d). These plots (Figures 5(d, e)) illustrate that a persistently exciting schedule pushes the training algorithm to converge closer to a robust minima.

Analysis of time complexity and memory overhead. Algorithm 1 maintains a $O(mn)$ time complexity which is negligible in comparison to the model training time (m, n are the number of values of hyperparameters M, N tried in Algorithm 1). Our primary increase in training time is a consequence of having to train a baseline model and then another model with a persistently exciting schedule. This results in a $2\times$ increase in time complexity. We hope future work can help boost performance (for example, by adapting learning rates online to satisfy PoE conditions). We also note that there is a small memory overhead in having to save gradients plus parameters after every epoch for use in Lipschitz estimation post training. This overhead is given by $O(n_{\text{epochs}}(n_{\text{params}} + n_{\text{pixels}}))$ where n_{epochs} , n_{params} , and n_{pixels} denote the number of epochs, model parameters and input image pixels respectively.

Limitations of the estimation algorithm. First, in training with few epochs (such as in the case of LeNet5 models with $N_{\text{epochs}} < 25$), adequate number of points of gradients and parameters for an accurate fit of a reverse Weibull distribution are not obtained. For this reason, we do not employ the estimation algorithm for LeNet5 but find the learning rates by analysis like in Section 5.2. For all the other models, this is not a limitation as they are each trained for 75 epochs to 300 epochs (more details in Appendix D). Further, this limitation is not an issue for modern deep learning where few-epochs training is rare or non-existent. Second, the estimation algorithm is inherently random because it depends on the gradients and parameters saved during the training process which can change with each run even when using the same random seed. Yet, the advantage of our results are that future work can introduce a better estimation algorithm (preferably with less inherent randomness) for \mathcal{L} and use it in conjunction with our scaled learning rate schedule for increased robustness.

C Details of Adversarial Training Frameworks and Autoattack

We describe the adversarial training frameworks analyzed in this work and the autoattack benchmark used to evaluate models trained in said frameworks below.

PGD-AT [Madry et al., 2017]

The general adversarial training min-max optimization problem is given by

$$\arg \min_{\theta} \mathbb{E}_{(X,Y) \in \mathcal{X} \times \mathcal{Y}} \left[\max_{\delta \in \mathbb{S}} L(h_{\Theta}(X + \delta), Y) \right] \quad (16)$$

where $\mathbb{S}_p = \{\delta \mid \|\delta\|_p < \epsilon\}$, X, Y represent batch training data & labels and the rest of the notation is defined in Section 3.1. We are primarily concerned with l_{∞} perturbations in this work which is why we have $\mathbb{S} = \mathbb{S}_{\infty}$. The inner maximization is solved by projected gradient descent (PGD) on the negative loss function (for K steps with α step size) to get an adversarial example rep-

resented as $X^{(K)} = X + \delta^{(K)}$. The perturbed data point in the $(t+1)$ -th step (*i.e.* $X^{(t+1)}$) is given by

$$X^{(t+1)} = \prod_{X+\mathbb{S}} (X^{(t)} + \alpha \operatorname{sgn}(\nabla_X L(h_\Theta(X^{(t)}), Y))) \quad (17)$$

with initialization $X^{(0)} = X + \delta^{(0)}$ where $\delta^{(0)}$ can be set to 0 or to any random point within \mathbb{S} . The latter case is called PGD with random initialization. The $\prod_{x+\mathbb{S}}$ denotes projecting perturbations of perturbed data points into the set \mathbb{S} .

TRADES [Zhang et al., 2019]

In TRADES, a theoretically motivated surrogate loss that balances the trade-off between standard and robust accuracy is minimized. The TRADES loss function is given by,

$$L_\Theta^{\text{TRADES}} = L(h_\Theta(X), Y) + \beta \max_{\delta \in \mathbb{S}} D_{\text{KL}}(h_\Theta(X + \delta) || h_\Theta(X)) \quad (18)$$

where D_{KL} represents Kullback–Leibler (KL) divergence and β is a hyperparameter that controls the aforementioned trade-off.

RST [Carmon et al., 2019]

In RST, a separate standard model is trained over CIFAR10 and used to generate pseudo-labels for unlabelled images from the Tiny Images dataset [Torralba et al., 2008]. Then a robust model is trained over the unlabelled data and its pseudo-labels by minimizing the TRADES loss given above. By this self-supervised training process, an adversarial-trained robust classifier is obtained.

Wide-RST [Wu et al., 2021]

Wide-RST augments RST with a wider model and larger value of hyperparameter β in the TRADES loss function. The choice of a wider model for increased robustness is theoretically motivated by Wu et al. [2021] and β is set to a larger value for improved perturbation stability.

Autoattack [Croce and Hein, 2020]

Autoattack consists of 4 attacks – Auto-PGD on cross entropy loss (white-box), Auto-PGD on difference of logits ratio loss (also white-box), Fast adaptive boundary attack (black-box) and Square attack (also black-box). Evaluation on autoattack has very little (0.01%) to no variance in different runs. Moreover, it has only one hyperparameter ϵ (usually set to 8/255) while all others are fixed and abstracted away from the evaluation making comparison across models and frameworks easy.

D Additional Experiment Details and Results

Our Code Our code and instructions can be found at the following github link: <https://github.com/kaustubhsridhar/PoE-robustness>.

Hyperparameters for Standard Training.

The CIFAR10 and CIFAR100 train sets consist of 50000 images and their validation sets have 10000 images. CIFAR10 has 10 classes while CIFAR100 has 100 classes.

For all ResNet (20, 50, 110) and DenseNet (40-12) models in standard training, we use a weight decay of $1e-4$ and a momentum value of 0.9. The train batch size was set to 128 for all ResNets and 64 for DenseNet-40-12. Further, no dropout is used. The total number of epochs (for training) and the details of the learning rate schedule are given in Tables 3 and 4 for CIFAR10 and CIFAR100 models respectively. All the hyperparameters were chosen from the corresponding PyTorch baseline.

Estimation parameters and learning schedules for Standard Training.

Following the certified estimation procedure in Appendix B, we obtain parameters M, N , estimate \mathcal{L}_{est} and initial learning rate η^1 for the baseline schedule, persistently exciting schedule and largest convergent schedule as given in Tables 3 and 4 for CIFAR10 and CIFAR100 models respectively. We also report the total number of epochs and remaining schedule description in Tables 3 and 4.

CIFAR10 Models	M	N	\mathcal{L}_{est}	η^1			Total epochs	Schedule
				base	$2/\mathcal{L}_{\text{est}}$	$1/\mathcal{L}_{\text{est}}$		
ResNet 20	200	100	3.526	0.1	0.5672	0.2836	164	divide by 10 at epochs 81 & 122
ResNet 50	200	164	10.79	0.1	0.1852	0.0926	164	divide by 10 at epochs 81 & 122
ResNet 110	200	164	11.70	0.1	0.1709	0.0855	164	divide by 10 at epochs 81 & 122
DenseNet 40	100	100	5.429	0.1	0.3683	0.1842	300	divide by 10 at epochs 150 & 225

Table 3: Standard training on CIFAR10: chosen parameters of \mathcal{L} estimation algorithm and corresponding \mathcal{L}_{est} and η^1 alongside learning rate schedules.

CIFAR100 Models	M	N	\mathcal{L}_{est}	η^1			Total epochs	Schedule
				base	$2/\mathcal{L}_{\text{est}}$	$1/\mathcal{L}_{\text{est}}$		
ResNet 50	200	164	8.75	0.1	0.2286	0.1143	164	divide by 10 at epochs 81 & 122
ResNet 110	200	164	14.48	0.1	0.1381	0.069	164	divide by 10 at epochs 81 & 122
DenseNet 40	100	100	7.30	0.1	0.274	0.137	300	divide by 10 at epochs 150 & 225

Table 4: Standard training on CIFAR100: chosen parameters of \mathcal{L} estimation algorithm and corresponding \mathcal{L}_{est} and η^1 alongside learning rate schedules.

Hyperparameters for Adversarial Training

We have the hyperparameters for adversarial training for all four approaches (PGD-AT, TRADES, RST, Wide-RST) in Table 5 below. The $\beta = 1/\lambda$ parameter is specific to the TRADES formulation of adversarial loss which is also used in RST and Wide-RST. It does not exist for the adversarial loss in PGD-AT. The same perturbation budget $\epsilon = 8/255$, attack steps = 10, and attack step-size of 0.007 are used in all methods. These hyperparameters are obtained from the current SOTA of the four frameworks as given in [Madry et al., 2017, Zhang et al., 2019, Carmon et al., 2019, Wu et al., 2021].

Approach	wd	momentum	train batch size	ϵ	attack steps	attack step-size	β
PGD-AT	5e-4	0.9	256	8/255	10	0.007	NA
TRADES	2e-4	0.9	128	8/255	10	0.007	6.0
RST	5e-4	0.9	256	8/255	10	0.007	6.0
Wide-RST	5e-4	0.9	256	8/255	10	0.007	21.0

Table 5: Adversarial training hyperparameters for each approach.

Estimation parameters and learning schedules for Adversarial Training

Following the certified estimation procedure in Appendix B, we obtain parameters M , N , estimate \mathcal{L}_{est} and initial learning rate η^1 for the SOTA schedule, persistently exciting schedule and largest convergent schedule as given in Table 6 below. We also report the total number of epochs and the remaining schedule description in Table 6. Both of these (total number of epochs and schedule) are obtained from the current SOTA of the four frameworks as given in [Madry et al., 2017, Zhang et al., 2019, Carmon et al., 2019, Wu et al., 2021]. The learning rate schedule in the SOTA implementations of PGD-AT [Madry et al., 2017] and TRADES [Zhang et al., 2019] is a step decay schedule. A cosine annealing schedule is used in the SOTA implementations of RST [Carmon et al., 2019] and Wide-RST [Wu et al., 2021] and is given by, $\eta(\text{epoch}) = \eta_{\min} + 0.5(\eta_{\max} - \eta_{\min}) \left(1 + \cos\left(\pi \frac{\text{epoch}}{\text{Total epochs}}\right)\right)$.

Approach	M	N	\mathcal{L}_{est}	η^1			Total epochs	Learning Rate Schedule
				SOTA	$2/\mathcal{L}_{\text{est}}$	$1/\mathcal{L}_{\text{est}}$		
PGD-AT	55	150	10.40	0.1	0.1922	0.0961	150	divided by 10 every 50 epochs
TRADES	99	25	7.497	0.1	0.2668	0.1334	75	divided by 10 at 75th epoch
RST	160	200	13.46	0.1	0.1485	0.0743	200	cosine annealing with $\eta_{\max} = \eta^1$, $\eta_{\min} = 0$
Wide-RST	160	200	13.46	0.1	0.1485	0.0743	200	cosine annealing with $\eta_{\max} = \eta^1$, $\eta_{\min} = 0$

Table 6: Adversarial training: chosen parameters of \mathcal{L} estimation algorithm and corresponding \mathcal{L}_{est} and η^1 alongside learning rate schedules.

Data Augmentation for Standard and Adversarial Training. Following the common practice for CIFAR datasets (and following the SOTA implementations of all 4 adversarial training frameworks), training images are augmented with random crops (padding by 4 pixels and cropping to 32×32) and random horizontal flips.

Code bases utilized. The code for LeNet5 on MNIST is based on <https://github.com/ChawDoe/LeNet5-MNIST-PyTorch> (No license). Standard training in CIFAR10, CIFAR100 for all models is based on code from a repository of PyTorch baselines at <https://github.com/bearpaw/pytorch-classification> (MIT license). We used the AdvTorch python library [Ding et al., 2019] at <https://github.com/BorealisAI/advtorch> (GNU general public license) for PGD implementation in standard training.

In adversarial training, the code for PGD-AT framework [Madry et al., 2017] is from <https://github.com/MadryLab/robustness> (MIT license), the code for TRADES [Zhang et al., 2019] framework is from <https://github.com/yaodongyu/TRADES> (MIT license) and the code for both RST [Carmon et al., 2019] and Wide-RST [Wu et al., 2021] frameworks is from <https://github.com/yaircarmon/semisup-adv> (MIT license). Our Lipschitz constant estimation code is based on previous work by Weng et al. [2018] and can be found at <https://github.com/huanzhang12/CLEVER> (Apache license).

Computation resources used in running experiments. We ran the experiments on either two Nvidia GeForce RTX 3090 GPUs (each with 24 GB of memory) or two Nvidia Quadro RTX 6000 GPUs (each with 24 GB of memory). The CPUs used were Intel Xeon Gold processors @ 3.00 GHz.

Another example of baseline, persistently exciting and largest convergent learning schedules

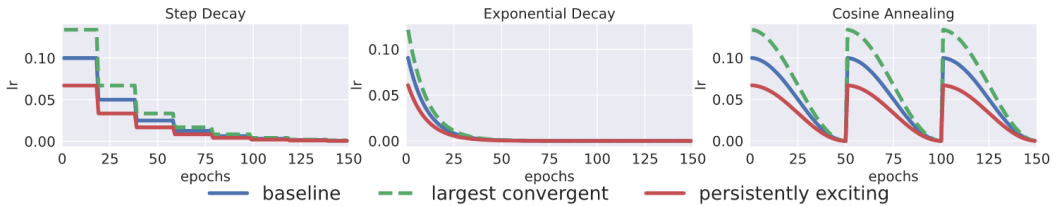


Figure 7: Second *e.g.* of baseline ($\eta^1 = 0.1$), largest convergent ($\eta^1 = 2/\mathcal{L}$) and persistently exciting ($\eta^1 = 1/\mathcal{L}$) schedules for three typical annealing strategies – step decay, exponential decay, and cosine annealing [Loshchilov and Hutter, 2016]. In this example, $\mathcal{L} = 15$ and persistently exciting schedule starts below baseline.

Magnified improvements with PoE and largest convergent schedule against 7-step PGD.

Dataset	Model	baseline	Largest Convergent $\eta^1 = 2/\mathcal{L}$	Persistently Exciting $\eta^1 = 1/\mathcal{L}$
CIFAR 10	ResNet 20	54.11	56.95	<u>56.76</u>
	ResNet 50	58.32	62.49	<u>61.57</u>
	ResNet 110	63.28	73.39	<u>64.9</u>
	DenseNet 40	43.43	42.2	45.22
CIFAR 100	ResNet 50	<u>23.28</u>	23.07	25.93
	ResNet 110	<u>30.62</u>	31.1	28.09
	DenseNet 40	<u>12.16</u>	13.54	<u>12.29</u>

Table 7: Standard trained models evaluated against a weaker 7-step PGD adversary with same perturbation budget $\epsilon = 1/255$ and step size $0.1/255$ as 20-step PGD. The number with the bold face and the underline denote the best and the second best result, respectively.

E A More Detailed Intuition Figure

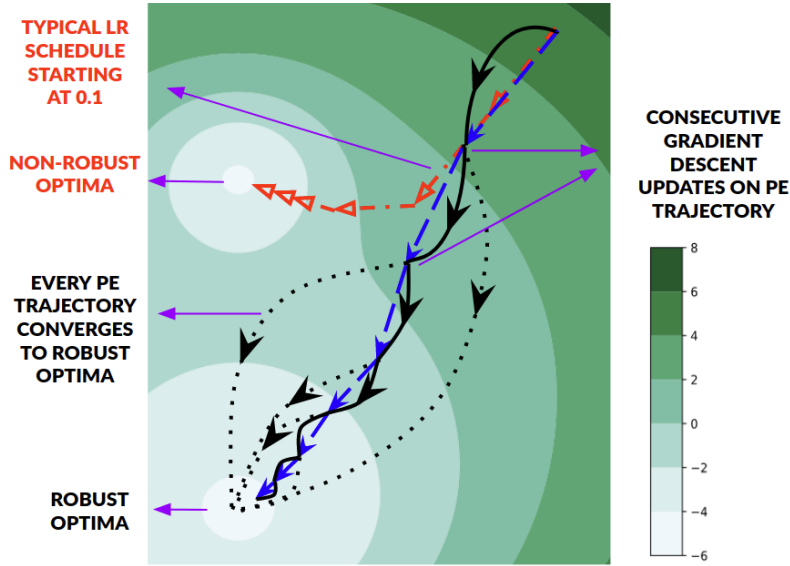


Figure 8: More Intuition: gradient descent updates (blue arrows) that lie on persistently excited trajectories (black curves with dotted extensions) go to robust optima (bottom). Each persistently excited trajectory, with sections possibly not on the loss surface, is guaranteed to converge exponentially-fast to the robust optima. A typical learning rate (lr) schedule starting at an initial value of 0.1 (red arrows) leads to local but not robust optima (top).